Coupled adhesion of bacteria to surfaces

Skogvold, Rebecca van der Westen

CHAPTER 3

Elastic and Viscous Bond Components in the Adhesion of Colloidal Particles and Fibrillated Streptococci to QCM-D Crystal Surfaces with Different Hydrophobicities using Kelvin-Voigt and Maxwell models

This chapter is published with permission from Royal Society of Chemistry:
Rebecca van der Westen, Prashant K. Sharma, Hans De Raedt, IJsbrand Vermue, Henny C. van der Mei and Henk J. Busscher[1]
Phys. Chem. Chem. Phys, **2017**, *19,* 25391–25400.

ABSTRACT

Quartz-crystal-microbalance with dissipation (QCM-D) can measure molecular mass adsorption as well as register adhesion of colloidal particles. However, analysis of QCM-D output to quantitatively analyze adhesion of (bio)colloids to obtain viscoelastic bond properties is still subject of debate. Here, we analyze the QCM-D output to analyze the bond between two hydrophilic streptococcal strains with 91-nm long and without fibrillar surface appendages and micron-sized hydrophobic polystyrene particles on QCM-D crystal surfaces with different hydrophobicities, comparing the Kelvin-Voigt and Maxwell model. A Poisson distribution was implemented in order to determine possible virtues of including polydispersity when fitting model parameters to the data. Quality of the fits did not indicate whether the Kelvin-Voigt or Maxwell model is preferential and only polydispersity in spring-constants improved the fit for polystyrene particles. Kelvin-Voigt and Maxwell models both yielded higher spring-constants for the bald streptococcus than for the fibrillated one. In both models, the drag coefficients increased for the bald streptococcus with the ratio of electron-donating over electron-accepting parameters of the crystal surface, while for the fibrillated strain the drag coefficient was similar on all crystal surfaces. Combined with the propensity of fibrillated streptococci to bind to the sensor crystal as a coupled-resonator above the crystal surface, this suggests that drag experienced by resonator-coupled, hydrophilic particles is more influenced by the viscosity of the bulk water than by interfacial water adjacent to the crystal surface. Hydrophilic particles that lack a surface tether are mass-coupled just above the crystal surface and accordingly probe a drag due the thin layer of interfacial water that is differently structured on hydrophobic and hydrophilic surfaces. Hydrophobic particles without a surface tether are also mass-coupled, but their drag coefficient decreases when the ratio of electron-donating over electron-accepting parameters increases, suggesting that hydrophobic particles experience less drag by structured water adjacent to a surface.

INTRODUCTION

The bond between colloidal particles adhering to a substratum surface is often considered rigid, but in reality consists of an elastic and a viscous component, which is especially the case when working with bio-colloids, like bacteria.[1] Bacteria can bind to surfaces through a variety of different surface appendages such as fibrils and fimbriae of various lengths,[2] adding to the viscoelasticity of the bond. The viscoelastic nature of the bacterium-substratum bond can be described by combinations of a linearly responding[3,4] spring and a dashpot, in which the spring represents the elasticity of the tether and the dashpot represents the viscous drag. Spring and dashpot can either be placed in parallel (Kelvin-Voigt model, see Figure 1a) or in series (Maxwell model, see Figure 1b). The dashpot slows down the response speed, generally referred to as damping.[5] Viscoelasticity of bacterial binding has been described as a means to allow bacteria more time to react in an appropriate way to catastrophic events, such as removal forces or chemical attack.[5,6]

The response kinetics of adhering bacteria to an applied stress differs considerably when the dashpot is placed in parallel with the spring (Figure 1a), damping any spring response or when both elements are placed in series (Figure 1b), allowing an immediate spring response followed by a delayed response due to the dashpot.[7] The viscoelastic response of adhering single bacteria under stress has been studied using Atomic Force Microscopy (AFM) and modeled to a one component Maxwell element.[1,8,9] Bacterial inhabitants in a biofilm adhere to a substratum surface and to each other and their stress response to low load compression[10,11] has been modeled using a series of Maxwell elements in parallel. Analysis of Brownian motion induced nanoscopic vibrations of single bacteria[12] and abiotic particles[13,14] adhering to substratum surfaces can also yield spring constants of binding tethers, but similar to AFM and optical tweezer-analyses[15] yields data that are accompanied by large standard deviations. This suggests a polydispersity of the binding tether characteristics. At the same time, the viscoelastic response of adhering bacteria or abiotic particles obtained employing a Quartz Crystal Microbalance with Dissipation (QCM-D) has been fitted with a phenomenological Kelvin-Voigt[16] or Maxwell model.[4]

The aim of this study is to compare the use of Kelvin-Voigt or Maxwell coupled resonator models in the analysis of the QCM-D response to adhesion of a fibrillated and non-fibrillated streptococcal strain. Abiotic polystyrene particles have been included for comparison, while QCM-D crystal surfaces have been applied possessing different hydrophobicities to determine whether either of the two models would be better applicable for particles adhering on a hydrophobic or hydrophilic surface. In addition, possible advantages of extending either phenomenological model with a polydispersity index are explored.

BACKGROUND ON QCM-D ANALYSIS

QCM-D is widely used in molecular adsorption. Per the conventional mass loading theory,[17] the adsorbed mass couples directly to the sensor surface (an AT-cut quartz crystal) increasing its effective mass, reducing its resonance frequency and leading to negative shifts in resonance frequency (Δf). Mass loading is mostly observed when molecular layers adhering to the sensor surface are thinner than 250 nm. The viscoelastic properties of the bond between an adhering mass and a substratum surface in the QCM-D can cause dissipation (ΔD). In contrast to molecular adsorption, colloidal particles adhere to the sensor surface via a tethered, non-rigid bond, causing positive frequency shifts, as schematically outlined in Figure 1c.[18–20] Positive frequency shifts can be explained[18] assuming adhering particles and the QCM-D crystal sensor act as coupled resonators.[16,21,22] The maximal energy dissipation change (ΔD) occurs when the particle resonance frequency (f_p) matches the crystal sensor resonance frequency (f_s). Moreover, the QCM-D can identify a zero-value in sensor resonance frequency shift (Δf_s) when particle and the crystal sensor resonance frequencies match, referred to as the frequency of zero-crossing (f_{ZC}) (see Figure 1c). Zero crossing frequencies can only be observed when occurring within the range of the sensor crystal resonance frequency and its overtones, usually between 5 and 65 MHz (see also Figure 1c).

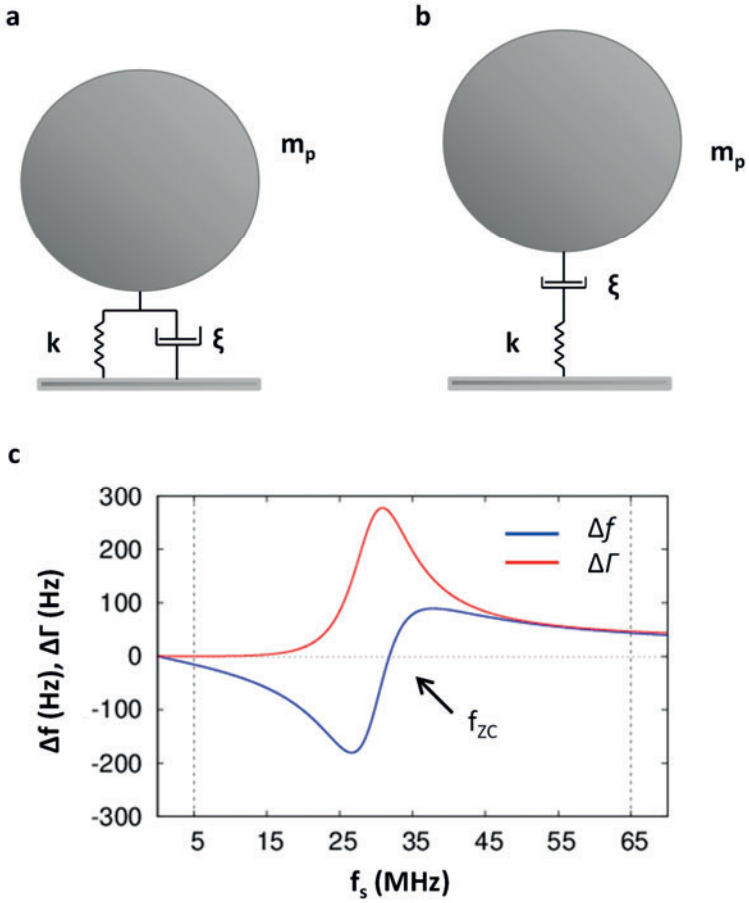

Figure 1. **a, b)** Mechanical equivalent circuit representing a particle with mass, m_p tethered to a surface via a viscoelastic bond containing a spring with spring constant (k) and a dashpot with a drag coefficient (ξ) in parallel (**a:** Kelvin-Voigt model) and in series (**b:** Maxwell model).

c) Schematic presentation of the shifts in resonance frequency and dissipation in QCM-D as a function of the crystal resonance frequency in a coupled resonator model according to Kelvin-Voigt. The frequency of zero crossing is chosen within the observable window of the sensor resonance frequency and its overtones at which the resonance frequencies of the crystal (f_s) and of the adhering particles (the particle resonance frequency f_p, taken here as 30 Hz) match. Input parameters for the generation of this graph according to Eq 1: f_F = 5 MHz, $m_p = 3 \times 10^{-16}$ kg, $\omega_p = 2\pi \times 30$ Hz, $\omega_s = 2 \pi \times f_s$, where f_s is in the range between 5 and 65 MHz, $Z_q = 8.8 \times 10^6$ kg m^{-2} s^{-1}), $N_p = 1.1 \times 10^{10}$ m^{-2}). Note: ΔΓ in Figure 1c is related to dissipation according to $\Delta\Gamma = \Delta D \times f_s/2$ (see data analysis section).

The elastic and viscous contributions to the bond can be evaluated by assuming the bond to be either Kelvin-Voigt or Maxwell in nature (Figure 1a or b) according to Eqs. 1[16] or 2,[4,7]respectively

$$\Delta f + \frac{i\Delta D f_s}{2} = \frac{f_F m_p}{\pi Z_q} \cdot N_p \left[\frac{\omega_s^3(\omega_p^2 - \gamma^2) - \omega_s \omega_p^4}{(\omega_s^2 - \omega_p^2)^2 + \omega_s^2 \gamma^2} + i \frac{\omega_s^4 \gamma}{(\omega_s^2 - \omega_p^2)^2 + \omega_s^2 \gamma^2} \right] \quad [1]$$

$$\Delta f + \frac{i\Delta D f_s}{2} = \frac{f_F N_p}{\pi Z_q} \cdot \left[i\omega_s m_p \frac{1}{1 - \frac{\omega_s^2}{\omega_p^2} + \frac{i\omega}{\gamma}} \right] \quad [2]$$

where ΔD is the shift in dissipation, f_F is the fundamental frequency of the crystal (5 MHz), m_p is the inertial mass of the particle in kg, ω_p is the resonance angular frequency for the particle, ω_s is the sensor angular frequency, Z_q is the acoustic impedance of an AT-cut quartz crystal (8.8 x 10^6 kg m^{-2} s^{-1}), N_p is the number of adhering particles per unit area (m^{-2}). Eqs. 1 and 2 can be simply derived using the basic QCM-D equation and inserting the mechanical analogues of the Kelvin-Voigt or Maxwell element. Since the QCM-D is a mechanical system, the rules for adding mechanical impedances differ from the rules for adding impedances in electricity: when mechanical elements operate in parallel, the total impedance is additive, opposite to when they operate in series in which case the inverse total impedance is the sum of the inverse impedance of the individual elements.[23]

γ, ω_p and m_p can be derived from Eqs. 1 or 2 for both models without accounting for polydispersity, using a brute-force, iterative procedure, as recently described for the Kelvin-Voigt model[24] and that can be analogously applied to the Maxwell model. As $\omega_p = \sqrt{k/m_p}$, the spring constant *k* can be directly calculated, while since $\gamma = \xi/m_p$ the drag coefficient, *ξ* immediately follows. Although the inertial mass m_p does not necessarily have to equal the gravitational mass of the particles, order of magnitude matching has been suggested for validation of physically realistic results of the brute-force, iterative procedure.[24]

In order to account for a possible polydispersity in inertial mass, spring constant and drag-force (m_p, k and ξ, respectively) as suggested by the large standard deviations in AFM, optical tweezer- and vibration analyses of colloidal bond characteristics, a Poisson distribution can be implemented into above Eqs. according to[25]

$$p(n, x) = \frac{\lambda^n e^{-\lambda}}{n!} \quad [3]$$

where *λ* indicates both the mean and variance of the distribution where n goes from 0 to N. In order to account for polydispersity, Eqs. 1 and 2 transform to 4

$$\Delta f + \frac{i\Delta D f_s}{2} = \frac{f_F N_p}{\pi Z_q}\{p(0,x)G(\omega_s, y_0, \omega_p, \gamma) + \{p(1,x)G(\omega_s, y_0(1+\delta), \omega_p, \gamma) + \{p(2,x)G(\omega_s, y_0(1+2\delta), \omega_p, \gamma) + \cdots + \{p(N,x)G(\omega_s, y_0(1+N\delta), \omega_p, \gamma)\} \quad [4]$$

where *G* corresponds to $\left[\frac{\omega_s^3(\omega_p^2-\gamma^2)-\omega_s\omega_p^4}{(\omega_s^2-\omega_p^2)^2+\omega_s^2\gamma^2} + i\,\frac{\omega_s^4\gamma}{(\omega_s^2-\omega_p^2)^2+\omega_s^2\gamma^2}\right]$ for inclusion of polydispersity in the Kelvin-Voigt model (Eq. 1) and to $\left[i\omega_s m_p \frac{1}{1-\frac{\omega_s^2}{\omega_p^2}+\frac{i\omega}{\gamma}}\right]$ for inclusion in the Maxwell model (Eq 2). In order to account for polydispersity in inertial mass, spring constant or drag coefficient, y_0 is chosen to be equal to either m_p, k or ξ, respectively, after which Eq. 4 can be used for fitting that accounts for polydispersities in either of the three above parameters m_p, k or ξ.

EXPERIMENTAL SECTION

Bacterial Strains, Culture Conditions and Harvesting. *Streptococcus salivarius* HB7 and HBC12 were used in this study. Both *S. salivarius* strains are hydrophilic, and negatively charged, but the two strains differ in their possession of surface appendages used to tether themselves to a substratum surface. *S. salivarius* HB7 possesses well-characterized 91 nm fibrils and *S. salivarius* HBC12 is devoid of surface appendages with a demonstrable length.[26] *S. salivarius* strains were pre-cultured in 10 mL of Todd Hewitt Broth (THB, OXOID, Basingstoke, UK) under static conditions, grown for 24 h at 37°C. After 24 h, pre-cultures were inoculated into 200 mL of THB and maintained under their above conditions for another 16 h. Bacteria were harvested by centrifugation at 5000 g for 5 min at 10°C and subsequently washed in 100 mL adhesion buffer (50 mM potassium chloride, 2 mM potassium phosphate, 1 mM calcium chloride, pH 6.8.). Next, bacteria were sonicated on ice 3 times for 10 s at 30 W (Vibra Cell Model 375; Sonics and Materials Inc., Danbury, CT) to maximize the number of single bacteria in suspension. Importantly for QCM-D experiments, bacteria were washed once more after sonication to remove any free molecules that might have been released during sonication to prevent molecular mass adsorption to the crystal sensor during bacterial adhesion. Finally, bacteria were diluted to a concentration of 3 x 10^8 bacteria per mL, as determined by counting in a Bürker-Türk chamber.

Abiotic Particles. Polystyrene particles (Bang Laboratories Inc. Fishers, IN, US), with a diameter of 1 µm similar as streptococci, were employed in this study in order to compare abiotic adhesion *versus* biotic particle adhesion. Prior to experiments, particles were washed twice by centrifugation in 10 mL ultrapure water, and diluted to a concentration of 2 x 10^8 particles per mL in 50 mM KCl.

Preparation of QCM-D Sensor Surfaces. 14 mm diameter, gold-coated quartz sensor crystals (Qsense, Gothenburg, Sweden) were cleaned prior to each experiment by immersion in a 3:1:1 mixture of ultrapure water (specific resistance > 18 MΩ cm), ammonia (NH_3) (Merck, Darmstadt, Germany) and hydrogen peroxide (H_2O_2) (Merck, Darmstadt, Germany) at 70°C for 15 min, followed by 15 min of UV/Ozone treatment. For QCM-D experiments, gold-coated sensor crystals were left for 24 h in a well-plate.

For coating the QCM-D crystal sensors with a hydrophobic self-assembled monolayer (SAM), crystals were left immersed in 0.001 M of 1-octadecanethiol dissolved in 100% ethanol for 18 h under mild shaking to obtain a homogenous coating. To obtain hydrophilic crystal sensors, crystals were immersed in 0.0001 M of 11-mercapto-1-undecanol (Sigma- Aldrich, Zwijndrecht, The Netherlands) in 100% ethanol under the above conditions.

Contact Angle Measurements. Contact angles were measured on differently coated crystal surfaces with three liquids possessing different polarities (water, formamide, and methyleneiodide), using a homemade goniometer. The contact angles were recorded by a fixed camera about 5 s after placing an 0.5 µL liquid droplet on a crystal surface. Three droplets of each liquid were randomly placed over one crystal surface, employing three different crystals for each measurement. The droplet contours were detected by grey-value thresholding and contact angles were calculated from the digitized contours using home-made software. Contact angles on each surface were converted to a Lifshitz-Van der Waals (γ^{LW}) and acid-base (γ^{AB}) surface free energy component, while the acid-base components were split up into an electron-donating (γ^-) and an electron-accepting (γ^+) parameter[27] according to

$$\begin{bmatrix} \sqrt{\gamma^{LW}_{water}} & \sqrt{\gamma^{+}_{water}} & \sqrt{\gamma^{-}_{water}} \\ \sqrt{\gamma^{LW}_{formamide}} & \sqrt{\gamma^{+}_{formamide}} & \sqrt{\gamma^{-}_{formamide}} \\ \sqrt{\gamma^{LW}_{methyleneiodide}} & \sqrt{\gamma^{+}_{methyleneiodide}} & \sqrt{\gamma^{-}_{methyleneiodide}} \end{bmatrix} \begin{bmatrix} \sqrt{\gamma^{LW}} \\ \sqrt{\gamma^{-}} \\ \sqrt{\gamma^{+}} \end{bmatrix} = \begin{bmatrix} (1+\cos\theta_{water}).\gamma_{water}/2 \\ (1+\cos\theta_{formamide}).\gamma_{formamide}/2 \\ (1+\cos\theta_{methyleneiodide}).\gamma_{methyleneiodide}/2 \end{bmatrix} \quad [5]$$

where γ^{LW} is the Lifshitz-Van der Waals surface free energy component and γ^- and γ^+ are the electron-donating and electron-accepting surface free energy parameters, respectively of the three liquids applied or the solid surface considered (see subscripts). The total surface free energy is denoted as γ, while θ represents the contact angles.

Surface Roughness Measurements by Atomic Force Microscopy (AFM). Surface roughnesses of the QCM-D crystal sensors, without coating and with hydrophobic or hydrophilic SAMs were measured using AFM in the contact mode with a silicon nitride cantilever tip (DNP from Bruker,

Woodbury, NY, USA). Each crystal sensor was imaged at three randomly chosen locations on the crystal surface and surface plots were generated in order to obtain a three-dimensional perspective of the surface, from which the surface roughness (R_a) was calculated (see Table 1).

QCM-D. All QCM-D experiments were carried out at room temperature using a window-equipped chamber (E1, Qsense, Gothenburg, Sweden). The window chamber containing the sensor crystal was mounted underneath a microscope (Leica DM2500 M, Rijswijk, The Netherlands) equipped with a CCD camera (Model A101, Basler vision technologies, Ahrensburg, Germany), enabling real-time monitoring of particulate adhesion on the QCM-D sensor surface. Frequency and dissipation shifts at 7 different sensor frequencies (5, 15, 25, 35, 45, 55 and 65 MHz) were acquired. Prior to particulate adhesion in the QCM-D, buffer was perfused through the chamber at a flow rate of 300 µL min^{-1} until a steady base line (variations in Δf less than 2 MHz over 5-10 min) was obtained.

Following this, a particulate suspension was perfused through the chamber at a flow rate of 300 µL min^{-1} for 1 h. Subsequently, buffer was perfused again to remove the particulate suspension from the QCM-D chamber, followed by the determination of the number of adhering particles per unit area.

Data Analysis. The frequency and dissipation shifts were retrieved from the QCM-D, as illustrated in Figure 2, and converted into Δf and ΔΓ, with $\Delta\Gamma = \Delta D \times f_s/2$. These values were then used to fit the data non-linearly to Eqs. 1 (Kelvin-Voigt model) or 2 (Maxwell model), using a brute-force, iterative algorithm, written in Python, to obtain parameters values for the spring constant (k), dashpot (ξ), mass of the particle (m_p), and the root mean square deviation (RMSD) of the resulting fit viz a viz the measured data.[24] Data presented are those yielding the lowest RMSD. A similar iterative algorithm was also used to solve Eq. 4 as the extended form of Eqs. 1 and 2 accounting for a polydispersity index λ for the inertial mass, spring constant and drag force (Eqs. 3 and 4) setting λ to 0 (no polydispersity), 2, 5 or 7 (high polydispersity). Polydispersity indices presented are those yielding the lowest RMSD.

RESULTS

Hydrophobicities of the QCM-D crystal surfaces were varied by the application of a hydrophobic and hydrophilic SAM, yielding a wide variation in water contact angle ranging from 17 to 90 degrees, including the gold-coated crystal with a water contact angle of 54 degrees (see Table 1). Water contact angles are not sufficient to characterize surface hydrophobicity however, since hydrophobicity is due either to low electron-donating or low electron-accepting surface free energy parameters, as can be calculated from the contact angles with three liquids, as also presented in Table 1. Whereas Lifshitz-Van der Waals surface free energy components of all three surfaces are fairly high, only the hydrophobic SAM demonstrates a zero acid-base surface free energy component. The absence of an acid-base surface free energy component is due to a zero electron-donating and electron

accepting parameter of the hydrophobic SAM, opposite to the gold-coated crystal surface and the hydrophilic SAM, possessing both non-zero electron-donating and electron-accepting surface free energy parameters. Accordingly, the ratio of electron-donating over electron-accepting parameters varies widely across the three surfaces (see also Table 1), indicative of different structuring of water molecules adjacent to the surface.[28] All crystal surfaces employed were extremely smooth in the nanoscale region, although the hydrophilic SAM layer demonstrated a less rough surface than the hydrophobic one (see also Table 1).

Table 1 Water contact angles, surface free energy components and parameters together with surface roughnesses of QCM-D crystal surfaces with a hydrophobic or hydrophilic SAM coating. Data represent averages with standard deviations over three droplets on three different crystals.

	Crystal with hydrophobic SAM	**Gold-coated crystal**	**Crystal with hydrophilic SAM**
CONTACT ANGLES (degrees)			
Water	90 ± 7	54 ± 3	17 ± 5
Formamide	27 ± 7	17 ± 1	0 ± 0
Methyleneiodide	48 ± 10	37 ± 4	38 ± 8
SURFACE FREE ENERGY COMPONENTS AND PARAMETERS (10^{-3} J m^{-2})			
γ	35 ± 6	55 ± 2	58 ± 0
γ^{LW}	35 ± 6	41 ± 2	40 ± 4
γ^{AB}	0 ± 0	13 ± 0	17 ± 7
γ^{-}	0 ± 0	15 ± 2	49 ± 3
γ^{+}	11 ± 5	3 ± 1	2 ± 1
γ^{-}/γ^{+}	0 ± 0	5 ± 2	25 ± 2
SURFACE ROUGHNESS BY AFM (nm)			
R_a	3.0 ± 0.4	3.4 ± 0.3	1.7 ± 0.1

Table 2 presents the number of bacteria and polystyrene particles that adhered to the crystal surfaces after 1 h of perfusing the QCM-D chamber with a particle suspension. Numbers were all in the order of 10^{10} m^{-2}, representing a surface coverage of around 1-10%, sufficiently low to avoid interactions between adhering particles during crystal oscillation. The fibrillated streptococcal strain *S. salivarius* HB7 adhered in similar numbers to all three crystal surfaces. The bald strain, *S. salivarius* HBC12, adhered equally well to the crystal surfaces as did *S. salivarius* HB7, with the exception of the hydrophilic SAM coated crystal to which it adhered in two-fold lower numbers than to the other crystal surfaces. Polystyrene particles adhered in similar number to all crystal surfaces, comparable with the number in which the bald streptococcal strain adhered to the hydrophilic crystal surface.

Table 2 The number of adhering streptococci and polystyrene particles per unit area (N_p m^{-2}) on crystal surfaces with different hydrophobicities. Data represents averages with standard deviations over three separate experiments, with separately grown bacterial cultures and differently prepared suspension.

Biocolloids and colloids	**Crystal surface**	**N_p ($x10^{10}$ m^{-2})**
S. salivarius HB7		
	Hydrophobic SAM	4.1 ± 0.6
	Gold-coated crystal	3.5 ± 0.4
	Hydrophilic SAM	4.2 ± 1.3
S. salivarius HBC12		
	Hydrophobic SAM	3.8 ± 1.4
	Gold-coated crystal	3.4 ± 0.4
	Hydrophilic SAM	2.0 ± 0.7
Polystyrene particles		
	Hydrophobic SAM	1.8 ± 0.7
	Gold-coated crystal	1.0 ± 0.2
	Hydrophilic	2.0 ± 0.3

An example of the raw QCM-D data as a function of time is presented in Figure 2 for *S. salivarius* HB7 adhering to a hydrophobic SAM coated crystal. Frequency as well as dissipation shifts vary over time and with the overtone frequency. Data such as presented in Figure 2 and Table 2, were inserted in phenomenological Kelvin-Voigt and Maxwell models, with and without accounting for polydispersity in the forthcoming parts of the Results section.

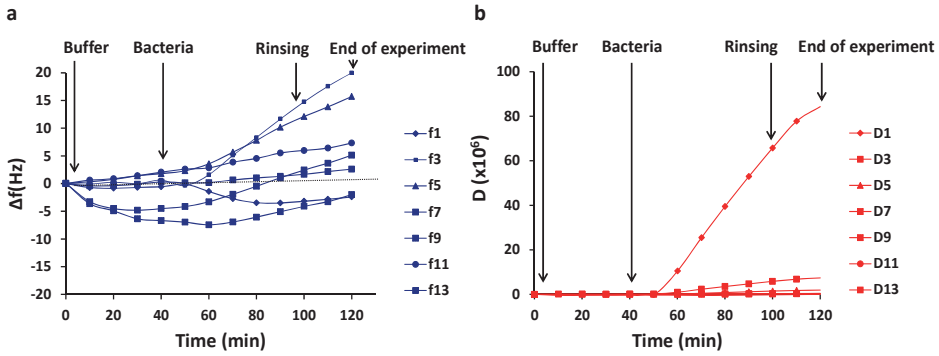

Figure 2. Example of the changes in frequency a), and dissipation b) as a function of time during adhesion of *S. salivarius* HB7 on hydrophobic SAM. f1 to f13 (a panel) and D1 to D13 (b panel) correspond to the different overtones frequencies ranging from 5 to 65 MHz. Note data points may be overlapping.

Figures 3, 4 and 5 show examples of the best fits of Kelvin-Voigt and Maxwell parameters for *S. salivarius* HB7, *S. salivarius* HBC12 and polystyrene particles under the experimental conditions specified, respectively, while Tables 3 and 4 summarize the resulting parameters after fitting the QCM-D output for streptococcal and polystyrene particle adhesion to the Kelvin-Voigt or Maxwell model, respectively.

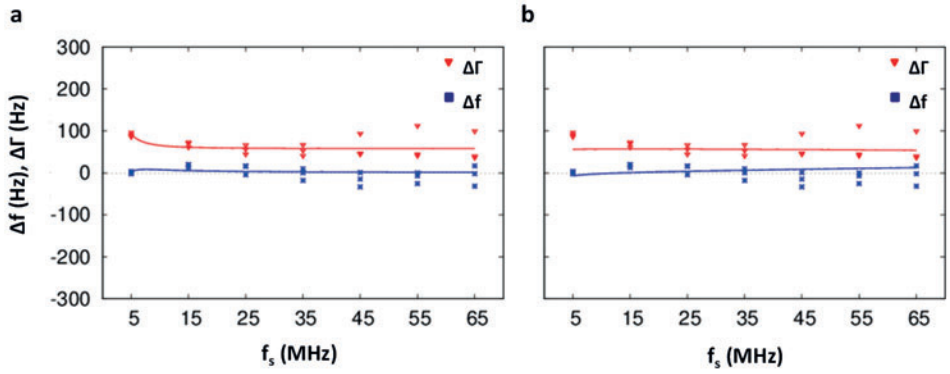

Figure 3. Examples of the QCM-D responses, Δf and ΔΓ for adhesion of *S. salivarius* HB7 to a hydrophobic SAM-coated crystal surface as a function of the sensor frequency in absence of a polydispersity index for a) the Kelvin-Voigt model and b) the Maxwell model.

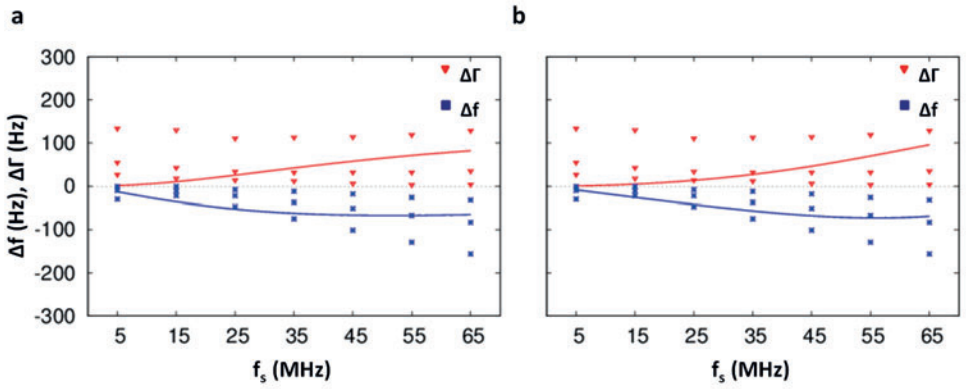

Figure 4. Examples of the QCM-D responses, Δf and ΔΓ for adhesion of *S. salivarius* HBC12 to a hydrophobic SAM-coated crystal surface as a function of the sensor frequency in absence of a polydispersity index for a) Kelvin-Voigt model and b) for the Maxwell model.

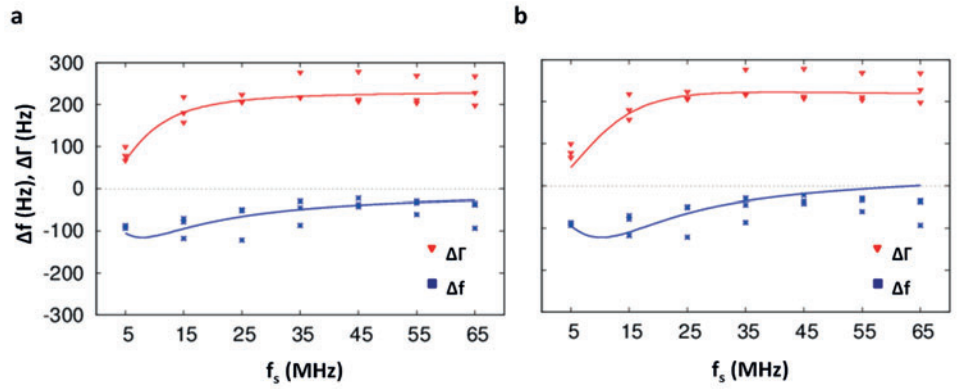

Figure 5. Examples of the QCM-D responses, Δf and ΔΓ for adhesion of polystyrene to a hydrophobic SAM crystal surface as a function of the sensor frequency for a) the Kelvin-Voigt model in absence of a polydispersity index and b) the Maxwell model in presence of a polydispersity index.

Fits for *S. salivarius* HB7 (Figure 3) consistently show a frequency of zero crossing (between 5 and 15 MHz) in line with Dybwad coupled resonator model, whereas *S. salivarius* HBC12 (Figure 4) and abiotic polystyrene particles (Figure 5) do not demonstrate frequencies of zero crossing, indicating the two particles behave more like an adsorbed mass rather than coupling as a resonator to the QCM-D crystal. The quality of the fits can be judged from the RMSD values in Tables 3 and 4. On average, RMSD values obtained using the Kelvin-Voigt model (43 ± 13 Hz) are similar as obtained from the Maxwell model (44 ± 11 Hz). The particle masses obtained for the biotic and abiotic particles range between 1 x 10^{-16} kg and 12 x 10^{-16} kg in the Kelvin-Voigt model, whereas in the Maxwell model particle masses between 1 x 10^{-16} kg and 20 x 10^{-16} kg are obtained. Therewith all masses obtained are within the same order of magnitude as can be calculated for bacteria (yielding 5 x 10^{-16} kg) from published bacterial

dimensions and densities or calculated from the dimension of the polystyrene particles and their density (yielding 5.5 x 10^{-16} kg).[29] For *S. salivarius* HBC12, both models yield an identical, small mass of 2 x 10^{-16} kg on average, while also for polystyrene particles both models yield a similar mass that is comparable with the gravitational mass of polystyrene particles. Interestingly, while both of these particles adhered more in line with mass adsorption theory, particle masses for *S. salivarius* HB7 that adhered more like a coupled resonator differ considerably as obtained from the Kelvin-Voigt (6 x 10^{-16} kg; see Table 3) *versus* the Maxwell model (20 x 10^{-16} kg; see Table 4).

Also spring constants *k* obtained from both models differ orders of magnitude for the three different particle types involved (compare Tables 3 and 4). In the Kelvin-Voigt model, the hydrophobicity of the crystal surface shows no systematic trend with the spring constant obtained, but in the Maxwell model the spring constants of *S. salivarius* HB7 and polystyrene particles were consistently smaller on the hydrophilic crystal surface.

Unlike the spring constants, but alike the particle masses obtained, both models yielded comparable results for the drag coefficients of mass-adsorbing *S. salivarius* HBC12 and abiotic polystyrene particles. The drag coefficients increased towards to the hydrophilic SAM coated crystals for the hydrophilic *S. salivarius* HBC12, while oppositely a decrease was observed for the hydrophobic polystyrene particles. For *S. salivarius* HB7 demonstrating coupled resonator characteristics, the drag coefficients obtained are comparable for both models and hardly vary among the different crystal surfaces.

Inclusion of polydispersity in mass, spring constant or drag-force for either bacterial strains did not increase the quality of the fit in Kelvin-Voigt nor in Maxwell models. However, for polystyrene particles in the Maxwell model inclusion of polydispersity in spring constant yielded a better fit than could be obtained in the absence of polydispersity or including polydispersity in mass or drag coefficient.

Table 3 Spring constants k, drag coefficients ξ masses m_p and RMSD values obtained in the Kelvin-Voigt coupled-resonator model, for both the fibrillated (*S. salivarius* HB7) and non-fibrillated (*S. salivarius* HBC12) streptococcal strains as well as for abiotic polystyrene particles. λ indicates the range of polydispersity to obtain best fit.

Bacterial strains	**m_p (10^{-16} kg)**	**k (kg s^{-2})**	**ξ (10^{-9} kg s^{-1})**	**λ**	**RMSD (Hz)**
S. salivarius HB7 on hydrophobic SAM	6	0.35	10	0	41
S. salivarius HB7 on gold-coated crystal	6	0.22	9	0	20
S. salivarius HB7 on hydrophilic SAM	5	0.24	5	0	84
S. salivarius HBC12 on hydrophobic SAM	1	0.00	19	0	42
S. salivarius HBC12 on gold-coated crystal	3	0.06	5	0	22
S. salivarius HBC12 on hydrophilic SAM	1	0.45	46	0	22
Polystyrene particles					
on hydrophobic SAM	12	0.00	61	0	39
on gold-coated crystal	5	0.00	113	0	64
on hydrophilic SAM	8	0.00	16	0	55

Table 4 Spring constants k, drag coefficients ξ masses m_p and RMSD values obtained in the Maxwell coupled-resonator model, for both the fibrillated (*S. salivarius* HB7) and non-fibrillated (*S. salivarius* HBC12) streptococcal strains as well as abiotic polystyrene particles. λ indicates the range of polydispersity to obtain best fit.

Bacterial strains	**m_p (10^{-16} kg)**	**k (kg s^{-2})**	**ξ (10^{-9} kg s^{-1})**	**λ**	**RMSD (Hz)**
S. salivarius HB7 on hydrophobic SAM	20	9.75	13	0	48
S. salivarius HB7 on gold-coated crystal	20	15.0	9	0	25
S. salivarius HB7 on hydrophilic SAM	20	2.10	13	0	80
S. salivarius HBC12 on hydrophobic SAM	0	15.0	21	0	44
S. salivarius HBC12 on gold-coated crystal	5	15.0	5	0	23
S. salivarius HBC12 on hydrophilic SAM	1	15.0	45	0	26
Polystyrene particles					
on hydrophobic SAM	10	554	79	2*	41
on gold-coated crystal	5	241	141	2*	58
on hydrophilic SAM	4	50.2	71	2*	51

* indicates polydispersity in *k*

DISCUSSION

Kelvin-Voigt and Maxwell models are both versatile instruments to model and explain the viscoelastic behavior of materials,[3] including biofilms.[5] This study compares the use of coupled resonator approaches based on phenomenological Kelvin-Voigt or Maxwell models and the possible role of polydispersity in the analysis of the QCM-D response to adhesion of a fibrillated and non-fibrillated streptococcal strain and abiotic polystyrene particles to QCM-D crystal surfaces having different hydrophobicities. The hydrophobicity of a gold-coated QCM-D crystal was varied by application of a hydrophobic or hydrophilic SAM, that differed not only in water contact angle, but moreover in the ratio between electron-donating and electron-accepting surface free energy parameters. All crystal surfaces were extremely smooth in the nanometer range (Table 1), although the hydrophilic SAM was slightly smoother than the two hydrophobic crystal surfaces Nevertheless, it is generally considered unlikely that such small nanoscopic differences in R_a will affect bacterial adhesion.[30]

QCM-D responses Δf and ΔΓ to the adhesion of biotic fibrillated streptococci and abiotic polystyrene particles could be fitted equally well using the Kelvin-Voigt or Maxwell model and comparison of RMSD values did not yield an indication as to which model might be preferentially used in the analysis of QCM-D responses from a mathematical perspective. Calculations of bacterial and polystyrene particle masses validate both phenomenological models within wide ranges, but it is uncertain to which extent the QCM-D yields actual gravitational or inertial masses and how the two relate.[16] Chindam et al.[3] marked the Kelvin-Voigt model as more accurate than the Maxwell model based on comparison with the Young's moduli obtained with its real value, but such "real" values for the bacterial properties are impossible to obtain. Comparison of the spring constants of bacterial bonds to substratum surfaces with independently obtained literature data is also difficult, not in the least since QCM-D operates at a forced, high frequency in the MHz range, whereas for instance bacterial vibration spectroscopy explores spring constants under naturally, Brownian motion induced, low frequency vibrations. Bacterial vibration spectroscopy indicated that the fibrillated streptococcal strain, *S. salivarius* HB7, had higher vibrational amplitudes than its bald mutant strain *S. salivarius* HBC12, corresponding with spring constants of around 2 and 3 x 10^{-5} N m^{-1}, respectively,[12] which is 5 orders of magnitude different than found here. Also spring constants obtained by means of AFM for whole cells, thus not specifically of the bond itself,[31,3] were orders of magnitude different than obtained here.

Herewith it becomes impossible to conclude which phenomenological model is mathematically or by comparison with other independent methods preferable. Such a conclusion at the same time may be less important than the question whether application of either model yields the same or different insights in the physico-chemistry of the bond underlying the phenomenon studied.

Both Kelvin-Voigt as well as Maxwell analyses, bacterial vibration spectroscopy and AFM of the streptococcal bonds point to a stiffer binding of the bald strain *S. salivarius* HBC12 than of the fibrillated *S. salivarius* HB7.[12] In neither QCM-D models, did inclusion of polydispersity yield a better quality of the fit for streptococcal adhesion. For polystyrene particles only a minor polydispersity ($\lambda = 2$) in spring constant was inferred. This suggests that polydispersity plays less of a role in the analysis of QCM-D responses to particle adhesion than proposed before.[16]

In both the Kelvin-Voigt and in the Maxwell analysis, the drag coefficient increases for the hydrophilic *S. salivarius* HBC12 going from the hydrophobic to the hydrophilic crystal surfaces, despite being numerically different in both analyses. These hydrophilic, biotic particles have no or very short surface appendages and concurrently, the QCM-D response suggests that these particles behave on the crystal surface as an adsorbed mass and may thus be more susceptible to the properties of the crystal surface and the resulting water structuring under the influence of the surface, as indicated by the high ratio of electron-donating over electron-accepting parameters on the hydrophilic SAM-coating. Oppositely for hydrophobic polystyrene particles in both models, the drag coefficient decreases when the ratio of electron-donating over electron-accepting parameters increases, suggesting that hydrophobic particles experience less drag by structured water on a surface than hydrophilic ones. The fact that the drag coefficient of *S. salivarius* HB7 is quite similar on hydrophilic and hydrophobic crystal surfaces combined with its propensity to bind to the sensor crystal as a coupled resonator, suggests that the drag coefficient of resonator coupled particles is much more influenced by the viscosity of the bulk water, i.e. far above the crystal surface than by the structured water adjacent to the crystal (note its fibrils are 91 nm long).

Separating the particle types involved in this study into mass adsorbing and resonator coupling ones, reveals an interesting difference between the Kelvin-Voigt and the Maxwell model. Whereas for *S. salivarius* HBC12 and polystyrene particles, particle masses derived are nearly the same in both models, *S. salivarius* HB7 has a fourfold higher mass in the Maxwell model than in the Kelvin-Voigt model. Pending the uncertainty regarding the proper mass (gravitational or inertial) derived in QCM-D and its "real" value, and the possible impact on the spring constants and drag coefficients derived, Johannsmann[4] suggested to use the ratio $\frac{\omega\xi}{k}$ or $\tan(\delta)$ as a "lossiness" parameter to be derived from QCM-D analyses, that is solely based on the ratio between the drag coefficients and spring constants of the bond.

Table 5 Lossiness tan(δ) obtained for both the fibrillated (*S. salivarius* HB7) and non-fibrillated (*S. salivarius* HBC12) streptococcal strains as well as for abiotic polystyrene particles in the Kelvin-Voigt and Maxwell model.

Bacterial strains	**tan(δ) Kelvin-Voigt**	**tan(δ) Maxwell**
S. salivarius HB7 on hydrophobic SAM	0.14	0.01
S. salivarius HB7 on gold-coated crystal	0.21	0.00
S. salivarius HB7 on hydrophilic SAM	0.11	0.03
S. salivarius HBC12 on hydrophobic SAM	>1	0.01
S. salivarius HBC12 on gold-coated crystal	0.41	0.00
S. salivarius HBC12 on hydrophilic SAM	0.51	0.01
Polystyrene particles		
on hydrophobic SAM	>1	0.00
on gold-coated crystal	>1	0.00
on hydrophilic SAM	>1	0.00

A summary of the "lossiness" values in Table 5 for both models yields the general conclusion that the Maxwell model yields predominantly elastic bond characteristics with minimal damping contributions. This can be explained by the fact that in the Kelvin-Voigt model the spring in parallel with the dashpot aids in particle movement (Figure 6a), whereas in the Maxwell model the spring and dashpot act completely independent of each other and the dashpot is not forced to participate in its response to the oscillations of the crystal by the spring (Figure 6b). Possibly this explains why the

Kelvin-Voigt model has been judged preferential above the Maxwell model in explaining the thermo-mechanical response of metals under elastic cyclic loading.[3] This may put larger emphasis on the elastic response in the Maxwell model compared with the Kelvin-Voigt model as suggested by the small "lossiness" values for the Maxwell model in Table 5. However, the fact that fluid is present all around the adhering particles and the bond itself is hydrated, indicates a necessary damping contribution to the bond, or lossiness, which the Kelvin-Voigt model allows for in contrast to the Maxwell model (see Table 5). This realization may also explain why *S. salivarius* HB7 has a fourfold higher mass in the Maxwell model than in the Kelvin-Voigt model, as the dashpot does not become activated by the spring to make the particle resonate in tune with the crystal through the bulk liquid. However, also two Maxwell elements placed in parallel, as often employed to model the viscoelastic response of biofilms,[5] with one being predominantly elastic and the other mainly viscous would in essence resemble the Kelvin-Voigt element and give the same response. For biofilms, it appears trivial that their viscoelastic response comprises too many independent processes for capturing in one Kelvin-Voigt or Maxwell element, but it cannot be ruled out that also the QCM-D response to single particle adhesion comprises multiple Maxwell elements that might pairwise resemble the Kelvin-Voigt element. Unfortunately, the use of multiple elements in analogy with the analysis of stress relaxation of biofilms for fitting the QCM-D response of adhering bacteria, is mathematically impossible due to the limited number of frequencies that can be observed in QCM-D.

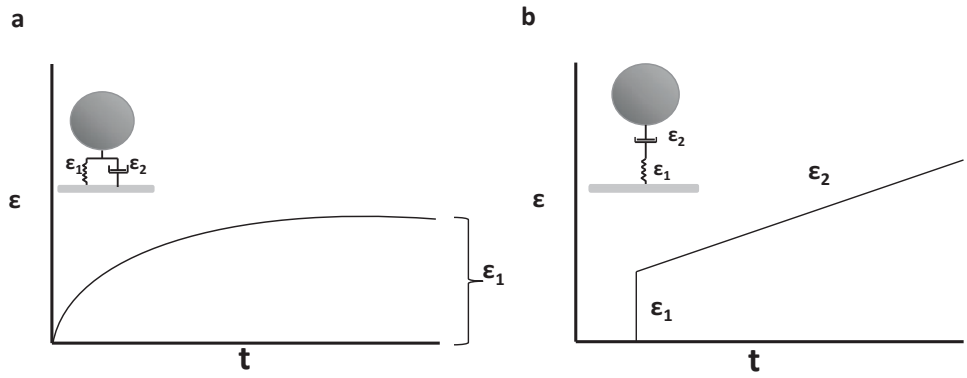

Figure 6. Schematic presentation of the strain of a bond in the Kelvin-Voigt (a) *versus* the Maxwell-model (b) as a function of time[7] during application of a constant stress, as experienced by adhering (bio)colloidal particles exposed to fluid shear.
a) The dashpot in parallel with the spring, dampens the spring response. The stretching continues to a plateau level. b) Spring and dashpot in series act independently. The spring immediately stretches to a constant strain, but the dashpot continues to stretch without being limited till ultimately the bond breaks.

CONCLUSION

In conclusion, we demonstrated a new way to quantitatively analyze QCM-D responses of (bio)colloid adhesion to hydrophobic and hydrophilic crystal surfaces to obtain viscoelastic bond properties. The use of a phenomenological Kelvin-Voigt or Maxwell model in a coupled-resonator approaches yielded good fits to the QCM-D data. Only inclusion of polydispersity in spring constant only improved the quality of the fits in the Maxwell model for hydrophobic polystyrene particles. In the Kelvin-Voigt and Maxwell model, the drag coefficient increased for the bald streptococcus with the ratio of electron-donating over electron-accepting parameters of the crystal surface, likely because it coupled closer to the crystal surface and more like an adsorbed mass than the fibrillated strain. For the fibrillated strain, the drag coefficient was similar on all crystal surfaces. Thus the drag experienced by resonator-coupled, hydrophilic particles is more influenced by the viscosity of the bulk water than by the structured water adjacent to the crystal surface that is probed by particles coupled without a tether, positioning the particle just above the thin interfacial layer of structured water on a surface.

Kelvin-Voigt and Maxwell models both have their virtues in analyzing the phenomenon of bacterial or particle adhesion when it comes to fitting of coupled resonator models to QCM-D data. Apart from the above conclusions that could be drawn on basis of both models, the Maxwell model in general emphasized the elastic response more than the Kelvin-Voigt model. Placed in series with a dashpot, the elastic response in the Maxwell model acts independently of damping. In the Kelvin-Voigt model, the spring is placed in parallel with the dashpot and continuously opposed in its response by the dashpot. Exposed to fluid shear, this implies that in the Maxwell model, the bond elongates till rupture, which is unrealistic and may make the Kelvin-Voigt model preferential.

ACKNOWLEDGEMENTS

We thank Dr. Philipp Kühn from the Department of Biomedical Engineering, Groningen, for performing the AFM measurements on QCM-D crystals.

FUNDING

This study was entirely funded by UMCG, Groningen, The Netherlands.

COMPETING INTEREST

The authors declare no potential conflicts of interest with respect to authorship and/or publication of this article. HJB is also director of a consulting company SASA BV. Opinions and assertions contained herein are those of the authors and are not construed as necessarily representing views of the funding organization or their respective employer(s).

REFERENCES

(1) Vadillo-Rodriguez, V.; Schooling, S. R.; Dutcher, J. R. *In Situ* Characterization of Differences in the Viscoelastic Response of Individual Gram-Negative and Gram-Positive Bacterial Cells. *J. Bacteriol.* **2009**, *191*, 5518–5525.

(2) Ramstedt, M.; Nakao, R.; Wai, S. N.; Uhlin, B. E.; Boily, J.-F. Monitoring Surface Chemical Changes in the Bacterial Cell Wall: Multivariate Analysis of Cryo-X-Ray Photoelectron Spectroscopy Data. *J. Biol. Chem.* **2011**, *286*, 12389–12396.

(3) Chindam, C.; Venkata, K. C.; Balasubramaniam, K.; Prakash, R. V. Thermomechanical Response of Metals: Maxwell vs. Kelvin–Voigt Models. *Mater. Sci. Eng.* **2013**, *560*, 54–61.

(4) Johannsmann, D. Towards Vibrational Spectroscopy on Surface-Attached Colloids Performed with a Quartz Crystal Microbalance. *Sens. Bio-Sensing Res.* **2016**, *11*, 86-93.

(5) Peterson, B. W.; He, Y.; Ren, Y.; Zerdoum, A.; Libera, M. R.; Sharma, P. K.; van Winkelhoff, A.-J.; Neut, D.; Stoodley, P.; van der Mei, H. C.; Busscher H. J. Viscoelasticity of Biofilms and Their Recalcitrance to Mechanical and Chemical Challenges. *FEMS Microbiol. Rev.* **2015**, *39*, 234–245.

(6) Shaw, T.; Winston, M.; Rupp, C. J.; Klapper, I.; Stoodley, P. Commonality of Elastic Relaxation Times in Biofilms. *Phys. Rev. Lett.* **2004**, *93*, 098102.

(7) Flügge, W. Viscoelastic Models. In *Viscoelasticity*; Prager, W., Kestin, J., Eds.; Blaisdell Publising company, **1967**,3–21.

(8) Francius, G.; Hemmerlé, J.; Ball, V.; Lavalle, P.; Picart, C.; Voegel, J. C.; Schaaf, P.; Senger, B. Stiffening of Soft Polyelectrolyte Architectures by Multilayer Capping Evidenced by Viscoelastic Analysis of AFM Indentation Measurements. *J. Phys. Chem. C* **2007**, *111*, 8299–8306.

(9) Vadillo-Rodriguez, V.; Beveridge, T. J.; Dutcher, J. R. Surface Viscoelasticity of Individual Gram-Negative Bacterial Cells Measured Using Atomic Force Microscopy. *J. Bacteriol.* **2008**, *190*, 4225–4232.

(10) He, Y.; Peterson, B. W.; Jongsma, M. A.; Ren, Y.; Sharma, P. K.; Busscher, H. J.; Van der Mei, H. C. Stress Relaxation Analysis Facilitates a Quantitative Approach towards Antimicrobial Penetration into Biofilms. *PLoS One* **2013**, *8*, e63750.

(11) Peterson, B. W.; Busscher, H. J.; Sharma, P. K.; Van der Mei, H. C. Visualization of Microbiological Processes Underlying Stress Relaxation in *Pseudomonas aeruginosa* Biofilms. *Microsc. Microanal.* **2014**, *20*, 912–915.

(12) Song, L.; Sjollema, J.; Sharma, P. K.; Kaper, H. J.; Van der Mei, H. C.; Busscher, H. J. Nanoscopic Vibrations of Bacteria with Different Cell-Wall Properties Adhering to Surfaces under Flow and Static Conditions. *ACS Nano* **2014**, *8*, 8457–8467.

(13) Dabros, T.; Warszynski, P.; Van de Ven, T. G. M. Motion of Latex Spheres Tethered to a Surface. *J. Colloid Interface Sci.* **1994**, *162*, 254–256.

(14) Kamiti, M.; Van de Ven, T. G. M. Measurement of Spring Constants of Polyacrylamide Chains Bridging Particles to a Solid Surface. *Macromolecules* **1996**, *29*, 1191–1194.

(15) Neuman, K. C.; Nagy, A. Single-Molecule Force Spectroscopy: Optical Tweezers, Magnetic Tweezers and Atomic Force Microscopy. *Nat. Methods* **2008**, *5*, 491–505.

(16) Olsson, A. L. J.; Van der Mei, H. C.; Johannsmann, D.; Busscher, H. J.; Sharma, P. K. Probing Colloid-Substratum Contact Stiffness by Acoustic Sensing in a Liquid Phase. *Anal. Chem.* **2012**, *84*, 4504–4512.

(17) Sauerbrey, G. Verwendung von Schwingquarzen Zur Wägung Dünner Schichten Und Zur Mikrowägung. *Zeitschrift für Physik*. **1959**, *155*, 206–222.

(18) Dybwad, G. L. A Sensitive New Method for the Determination of Adhesive Bonding between a Particle and a Substrate. *J. Appl. Phys.* **1985**, *58*, 2789–2790.

(19) Johannsmann, D. Viscoelastic Analysis of Organic Thin Films on Quartz Resonators. *Macromol. Chem. Phys.* **1999**, *516*, 501–516.

(20) Pomorska, A.; Shchukin, D.; Hammond, R.; Cooper, M. A.; Grundmeier, G.; Johannsmann, D. Positive Frequency Shifts Observed upon Adsorbing Micron-Sized Solid Objects to a Quartz Crystal Microbalance from the Liquid Phase. *Anal. Chem.* **2010**, *82*, 2237–2242.

(21) Johannsmann, D. Viscoelastic, Mechanical, and Dielectric Measurements on Complex Samples with the Quartz Crystal Microbalance. *Phys. Chem. Chem. Phys.* **2008**, *10*, 4516–4534.

(22) D'Amour, J. N.; Stålgren, J. J. R.; Kanazawa, K. K.; Frank, C. W.; Rodahl, M.; Johannsmann, D. Capillary Aging of the Contacts between Glass Spheres and a Quartz Resonator Surface. *Phys. Rev. Lett.* **2006**, *96,* 058301.

(23) Firestone, F. A.; Firestong, B. F. A. A new analogy between mechanical and electrical systems. *J. Acoust. Soc. Am.* **1933**, *4*, 249.

(24) Van der Westen, R.; Van der Mei, H. C.; De Raedt, H.; Olsson, A. L. J.; Busscher, H. J.; Sharma, P. K. Quantification of the Viscoelasticity of the Bond of Biotic and Abiotic Particles Adhering to Solid-Liquid Interfaces Using a Window-Equipped Quartz Crystal Microbalance with Dissipation. *Colloids Surfaces B Biointerfaces* **2016**, *148*, 255–262.

(25) Evans, M.; Hastings, N.; Peacock, B. *Statistical Distributions*; 2000; Vol. 2.

(26) Van der Mei, H. C.; Leonard, A. J.; Weerkamp, A. H.; Rouxhet, P. G.; Busscher, H. J. Surface Properties of *Streptococcus salivarius* HB and Nonfibrillar Mutants: Measurement of Zeta Potential and Elemental Composition with X-Ray Photoelectron Spectroscopy. *J. Bacteriol.* **1988**, *170*, 2462–2466.

(27) Logofatu, C.; Negrila, C. C.; Ghita, R. V; Ungureanu, F.; Cotirlan, C.; Manea, C. G. A. S.; Lazarescu, M. F. Study of SiO 2 / Si Interface by Surface Techniques. *Cryst. Silicon - Prop. Uses Ed. by Prof. Sukumar Basu* **2011**, *1*, 2–42.

(28) Van Oss, C. J.; Giese, R. F. Role of the Properties and Structure of Liquid Water in Colloidal and Interfacial Systems. *J. Dispers. Sci. Technol.* **2004**, *25*, 631–655.

(29) Godin, M.; Bryan, A. K.; Burg, T. P.; Babcock, K.; Manalis, S. R. Measuring the Mass, Density, and Size of Particles and Cells Using a Suspended Microchannel Resonator. *App. Phys. lett.* **2007**, *91*, 1-3

(30) Truong, V. K.; Lapovok, R.; Estrin, Y. S.; Rundell, S.; Wang, J. Y.; Fluke, C. J.; Crawford, R. J.; Ivanova, E. P. The Influence of Nano-Scale Surface Roughness on Bacterial Adhesion to Ultrafine-Grained Titanium. *Biomaterials* **2010**, *31*, 3674–3683.

(31) Méndez-Vilas, A.; Gallardo-Moreno, A. M.; González-Martín, M. L. Atomic Force Microscopy of Mechanically Trapped Bacterial Cells. *Microsc. Microanal.* **2007**, *13*, 55–64.

(32) Yao, X.; Walter, J.; Burke, S.; Stewart, S.; Jericho, M. H.; Pink, D.; Hunter, R.; Beveridge, T. J. Atomic Force Microscopy and Theoretical Considerations of Surface Properties and Turgor Pressures of Bacteria. *Colloids Surfaces B Biointerfaces* **2002**, *23*, 213–230.